RSC Applied Interfaces

ROYAL SOCIETY OF CHEMISTRY

PAPER

View Article Online
View Journal | View Issue

Cite this: *RSC Appl. Interfaces*, 2025, **2**, 715

Wettability studies of LiCl-KCl and FLiNaK on metal and non-metal substrates

Qiufeng Yang, * Michael E. Woods and Ruchi Gakhar*

This study examines the wettability characteristics of molten LiCl-KCl and LiF-NaF-KF (FLiNaK) salts on a variety of metal and non-metal substrates, including C276, stainless steel 304 (SS 304), stainless steel 316 (SS 316), Alloy 617, molybdenum (Mo), nickel (Ni), tantalum (Ta), IG110, glassy carbon, MACOR and quartz, which are relevant for applications in molten salt reactors (MSRs) and differential scanning calorimetry (DSC) analysis. Contact angle measurements were conducted from room temperature up to 700 °C using the sessile drop method, revealing increased wettability of both salts as temperature increases. For LiCl-KCl tests, the contact angles on each substrate are in descending order as follows: $\theta_{IG110} > \theta_{glassy\ carbon} > \theta_{Mo} > \theta_{SS\ 304} > \theta_{C276} > \theta_{MACOR} > \theta_{SS\ 316} > \theta_{Alloy\ 617} > \theta_{quartz} \approx \theta_{Ni} > \theta_{Ta}$. For FLiNaK, the measured contact angles follow a similar trend: $\theta_{IG110} > \theta_{SS\ 304} > \theta_{quartz} > \theta_{C276} > \theta_{SS\ 316} > \theta_{Ta}$. The wetting of FLiNaK on the same substrate tends to be higher than that of LiCl-KCl, likely due to the larger surface tension between LiCl-KCl and substrates. The work of adhesion calculated from the contact angles shows an increase in adhesion force with increasing temperature for most substrates, indicating stronger contact between the salts and substrates. Contact angle is shown to be correlated with the corrosion resistance of pure metals, but this correlation is not observed in alloys due to their complex chemical compositions. The application of contact angle in the selection of DSC container materials is also suggested to ensure proper contact and uniform thickness.

Received 15th January 2025,
Accepted 7th February 2025

DOI: 10.1039/d5lf00007f

rsc.li/RSCApplInter

1. Introduction

Molten salts are increasingly recognized as promising heat exchanger media across various energy systems, attributed to their relatively high heat capacities, large thermal conductivities and low vapor pressures.[1–4] Specifically, molten chloride salts are excellent heat transfer fluids and thermal energy storage fluids for concentrated solar power plants.[5–7] The application of molten salts also extends to nuclear technologies, where $MgCl_2$-NaCl-KCl is utilized as solvent salt to separate americium from plutonium, and LiCl-KCl is applied as the solvent medium for electrorefining uranium in the pyroprocessing process.[8,9] Moreover, molten salts have been proposed as outstanding coolant and fuel salt candidates in MSRs, due to their neutron moderation properties and high chemical stability even under irradiation.[10] Their roles in nuclear fuel reprocessing and advanced reactor designs underscore the importance of understanding their thermophysical properties including melting point, vapor pressure, heat capacity and thermal conductivity. To obtain reliable thermophysical values from commonly used approaches such as DSC, it is crucial that the sample maintains proper contact with the sample container and does not exhibit strong wettability.[11] Improper contact can lead to a non-uniform melt thickness and inaccurate measurements. Molten salts may even creep up the heating container walls, further affecting the accuracy of the data. Therefore, studying the interfacial contact of molten salts on different substrates is essential to identify appropriate materials for use as salt containers in DSC measurements. Furthermore, structural material corrosion has been one of the major concerns in the application of molten salts.[12] Corrosion begins at the interface of structural materials and molten salts, involving mass transfer of impurities and corrosion products, and electron exchange between the bulk salt and the structural material.[13] Strong wetting correlates with enhanced surface interactions, indicating a higher potential of salt attack on the contacted material, thus prompting more corrosion.[14,15] This suggests that the molten salt corrosion resistance of certain materials can be predicted by directly measuring contact angles.

A contact angle less than 90° indicates high wettability, while a contact angle greater than 90° indicates low wettability.[16] Traditional methods to measure contact angle include the sessile drop, needle, tilting, captive bubble, Wilhelmy plate, meniscus, and Washburn methods, with the sessile drop method being the simplest and most widely used for optical

Advanced Technology of Molten Salts (ATOMS), Idaho National Laboratory, 1955 N Fremont Ave, Idaho Falls, ID, 83415, USA. E-mail: qiufeng.yang@inl.gov, ruchi.gakhar@inl.gov

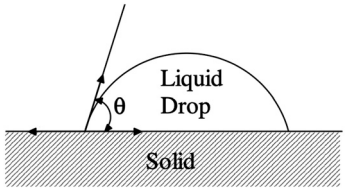

Fig. 1 Illustration of sessile drop method, θ is contact angle.

measurement of contact angle through drop shape analysis.[17] In the sessile drop method, contact angles are determined by applying tangents at the intersection of the drop outline as shown in Fig. 1. The accuracy of contact angle measurement is influenced by factors such as the size of the liquid drop and determination of the baseline at the interface.

The measurement of contact angle has been widely employed in various fields including coating development, surface treatment evaluation, and cleaning process optimization in aqueous solutions at room temperature.[18–23] However, studies available on molten salts at high temperatures remain scarce. Xu *et al.* studied the impregnation behavior of molten 2LiF-BeF_2 salt into a graphite matrix.[24] The measured contact angle was about 135°, indicating the non-wetting characteristics of the molten salt on this substrate. Deepika *et al.* investigated the wettability and corrosion of microgroove-patterned SS 304, revealing that the groove-shaped textured specimen was hydrophobic and exhibited superior anti-wetting behavior.[25] The micro-patterned surfaces also demonstrated excellent corrosion resistance due to the presence of air gaps between ridges and channels which impeded the corrosion. Delmore *et al.* studied the wettability of different types of graphite (A3, IG110 and CGB) with FLiBe and FLiNaK. The contact angles for FLiBe and FLiNaK were reported to be affected by porosity and structure of the different grades of graphite.[26] Grosu *et al.* investigated the wettability of molten $NaNO_3$-KNO_3 salts at 300 °C on multiple substrates.[11] It was found that the contact angles on materials such as magnesium, zinc and silver with a low surface energy were higher than 90°. Thus, using a crucible made of low surface energy material was one of the strategies proposed to control molten salt creeping in DSC measurements. Baumli *et al.* explored the wettability of graphite and glassy carbon in the presence of pure molten alkali chlorides (NaCl, KCl, RbCl, CsCl) using the sessile drop method.[27] The contact angle was found to decrease with increasing radius of the metal cation of salts. The adhesion energy between the carbon substrate and molten salt increased with the square of the radius of the cation and inversely decreased as the radius of the anion decreased.

Nevertheless, no comprehensive comparative studies have been conducted on the wettability behavior of LiCl-KCl and FLiNaK. To address this gap, this study measured the contact angle and calculated the work of adhesion for LiCl-KCl and FLiNaK on various substrates, including C276, SS 304, SS 316, Alloy 617, Mo, Ni, Ta, IG110, glassy carbon, MACOR and quartz. These materials are either candidates for salt-facing structural material in MSRs or salt container candidates in DSC measurements. The conventional sessile drop method was used for contact angle measurements and the trends of contact angle and work of adhesion with temperature were ascertained. This extensive database of wettability characteristics of LiCl-KCl and FLiNaK will benefit the selection of structural materials compatible with molten salts, the development of advanced corrosion-resistant coatings, and the optimization of the selection of salt container materials for DSC analysis.

2. Experimental

2.1. Materials

LiCl-KCl eutectic salt mixture (anhydrobeads, 99.99%, trace metal basis, 58.01 mol% LiCl), LiF (99.99%, trace metal basis), NaF (99.99%, trace metals basis), and KF (99.97%, trace metal basis) were procured from Sigma-Aldrich and stored in an argon-filled glovebox with $O_2 < 0.1$ ppm and $H_2O < 0.1$ ppm. The FLiNaK salt mixture was fabricated in the laboratory with a composition of 46.5 mol% LiF, 11.5 mol% NaF, and 42 mol% KF. A digital balance with an accuracy of 10^{-4} g was used to weigh the salt. The weighed salts were placed and mixed well in a glassy carbon crucible. Considering the strong hydrophilicity of salts, especially KF, the prepared salt mixtures were thermally purified by baking at different temperatures as suggested in the literature.[28] A calibrated muffle furnace with an accuracy of ±2 °C was used to heat the salts at each target temperature. LiCl-KCl underwent the same thermal purification process to eliminate the possible oxygen or moisture contamination from the transportation or storage process. The purified molten FLiNaK and LiCl-KCl salt mixtures were cooled to room temperature, broken into chunks, and sealed in glass vials for contact angle tests.

Given that surface roughness may influence wetting behavior, the metal substrates used in the tests—including Mo, C267, SS 304, SS 316, Alloy 617, Ni, and Ta—were all prepared with an identical surface finish. The metal substrates were polished with sandpapers ranging from 400 to 2400 grit, then finished with 1 um diamond polishing paste. The non-metal substrates—including IG 110, glassy carbon, MACOR and quartz—were used as received with no further polishing. All substrates were cleaned using deionized water and ethanol, followed by drying under vacuum at 120 °C prior to contact angle tests.

2.2. Experimental setup

The contact angle test apparatus as shown in Fig. 2 was placed inside an inert atmosphere glovebox. A room-temperature contact angle goniometer, Ossila L2004A1, was procured from Ossila and modified for high-temperature molten salt application. A custom heating stage, with dimensions of 6 cm in length, 3 cm in width, and 2 cm in height, was installed between the camera and backlight of the Ossila goniometer. The heating stage comprised a stainless-steel block featuring two holes bored to accommodate a K-type thermocouple and a

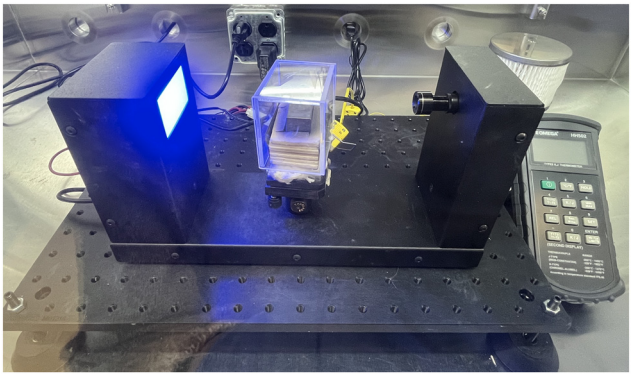

Fig. 2 Experimental apparatus for contact angle measurements: Ossila goniometer modified with a custom heating stage.

24-volt, 100-watt cartridge heater (Dalton W2C012). The stage was connected to a BK Precision DC power supply, allowing for manual control of the cartridge heater. The stage was heated to a target temperature with temperature monitoring provided by the thermocouple. Additionally, the stage was surrounded by insulation and a transparent quartz enclosure was placed over it to minimize heat loss and insulate the sample environment. The Ossila L2004A1 was equipped with an LED light and high-resolution camera connected to a computer, allowing for real-time image capture through the Ossila contact angle software. Prior to data collection, the stage was leveled using a bubble level. A small salt chunk, weighing approximately 10 mg, was placed in the center of the substrate surface, and the goniometer camera was focused. The initial target heating temperature was set to the melting point of the salt to avoid overheating. The temperature was then gradually increased to each successive target temperature. Given that the designed operating temperatures of MSRs range from 550 °C to 700 °C, the upper limit of temperature in the contact angle measurements was maintained within 700 ± 10 °C. Salt droplet images were captured from room temperature until the contact angle stabilized or salts completely wetted the substrate. Furthermore, prior to capturing a droplet image at each temperature, it was confirmed that the temperature variation was within ±2 °C for 30 min to ensure thermal equilibrium. ImageJ and Ossila contact angle analysis software were used to analyze the data. The contact angle of each test was ascertained by averaging the measured left and right contact angles. Ideally, the measured left and right value should be identical. However, due to various experimental factors such as stage leveling, potential impurities in the salts, substrate surface roughness, and uneven temperature distribution within salt samples, slight discrepancies between the left and right contact angles were observed. Consequently, the standard deviation of each measured contact angle was also calculated.

3. Results

Representative LiCl-KCl salt droplet images captured on the SS 304 substrate during the contact angle measurements are shown in Fig. 3. Table 1 summarizes the measured contact angles of LiCl-KCl and FLiNaK on various substrates at different temperatures, ranging from the initial fully molten temperature of the salts to the temperature at which the contact angle stabilized or the salts completely wetted the substrate. It should be noted that, although the melting points of LiCl-KCl and FLiNaK salts are reported to be 352 °C and 454 °C, respectively, the observed fully molten temperatures of the salts in the present study were slightly higher (367 °C to 429 °C for LiCl-KCl and 458 °C to 484 °C for FLiNaK). This deviation was likely due to the different thermal conductivities of substrates, and the temperature offset between the heating stage and the salt samples, despite the implementation of appropriate insulation. A more advanced heating stage design is needed to achieve more accurate temperature recording in future studies.

The trends of contact angle with temperature for LiCl-KCl are depicted in Fig. 4(a) and (b). The measured contact angles of LiCl-KCl on various substrates are generally arranged in the following sequence: $\theta_{IG110} > \theta_{glassy\ carbon} > \theta_{Mo} > \theta_{SS\ 304} > \theta_{C276} > \theta_{MACOR} > \theta_{SS\ 316} > \theta_{Alloy\ 617} > \theta_{quartz} \approx \theta_{Ni} > \theta_{Ta}$. For metal substrates, the measured contact angles on Mo were the largest, indicating its relatively low wettability with a contact angle of 108.6° at 376 °C. The measured contact angles on Ta were the smallest, exhibiting high wettability across all studied temperatures, with contact angles ranging from 25.25° at 367 °C to 11° at 404 °C. LiCl-KCl demonstrated the potential to completely wet the surfaces of Ta, Ni and Alloy 617 starting at 404 °C, 506 °C and 617 °C, respectively, with small contact angles of 11°, 10.3° and 2.31°. Complete wetting was not observed for Mo, C276, SS 304 and SS 316 across the temperature range examined in this study.

For the alloys, although Ni is the major or sole component of Ni, Alloy 617 and C276, the observed wettability characteristic of LiCl-KCl on these substrates varied slightly. The contact angles measured on C276 were the largest followed by Alloy 617, with pure Ni having the smallest values

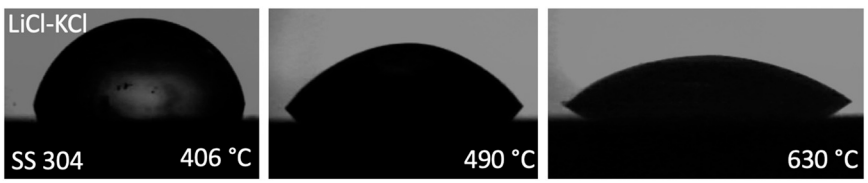

Fig. 3 Representative LiCl-KCl salt droplet images captured on the SS 304 substrate at different temperatures.

Table 1 Measured contact angle with standard deviation of LiCl-KCl and FLiNaK on various substrates at different temperatures

Contact angle of LiCl-KCl

Material	T (°C)	Contact angle (°)	Material	T (°C)	Contact angle (°)	Material	T (°C)	Contact angle (°)
Mo	376	108.60 ± 4.53	Ta	367	25.25 ± 1.48	MACOR	425	58.20 ± 0.28
	413	104.70 ± 3.25		378	18.25 ± 0.50		450	49.55 ± 0.49
	462	81.35 ± 3.46		389	13.50 ± 0.00		477	30.00 ± 1.70
	503	54.90 ± 4.24		396	12.05 ± 1.06		522	24.70 ± 0.71
	543	55.55 ± 2.33		404	11.00 ± 2.12		573	11.50 ± 2.10
	587	52.00 ± 3.11	SS 316	407	47.45 ± 0.78	Glassy carbon	381	101.27 ± 6.70
	630	45.00 ± 3.68		444	24.80 ± 1.56		459	91.25 ± 5.30
SS 304	406	79.35 ± 1.91		489	23.45 ± 1.63		480	87.35 ± 3.18
	444	70.40 ± 0.14		539	23.70 ± 3.68		506	76.10 ± 1.84
	490	52.10 ± 0.85		583	23.65 ± 3.46		530	71.30 ± 1.27
	531	48.70 ± 1.98	Ni	385	41.40 ± 4.53		556	72.65 ± 1.63
	585	48.65 ± 0.21		405	28.20 ± 3.68		583	72.55 ± 0.35
	630	38.20 ± 5.23		430	22.85 ± 2.90	Quartz	421	22.15 ± 1.48
	672	29.40 ± 2.26		455	17.95 ± 0.21		470	17.10 ± 1.27
	711	20.20 ± 1.41		481	13.45 ± 0.35		518	11.70 ± 3.96
C276	381	83.20 ± 2.69		506	10.30 ± 3.39		564	7.10 ± 0.85
	408	79.35 ± 3.74	Alloy 617	429	49.95 ± 0.46		615	11.95 ± 3.61
	432	42.75 ± 0.49		444	20.65 ± 0.18		660	6.50 ± 4.10
	455	39.65 ± 2.90		453	22.15 ± 0.39	IG 110	407	119.45 ± 1.91
	478	39.10 ± 1.13		465	22.10 ± 0.35		508	116.60 ± 4.10
	504	40.20 ± 1.41		489	21.75 ± 0.18		554	118.55 ± 2.62
	573	38.85 ± 1.06		569	22.45 ± 0.39		598	118.20 ± 3.25
	603	3.90 ± 1.84		617	2.31 ± 1.39		645	119.45 ± 3.46
							692	118.20 ± 5.37

Contact angle of FLiNaK

Material	T (°C)	Contact angle (°)	Material	T (°C)	Contact angle (°)	Material	T (°C)	Contact angle (°)
C276	467	30.10 ± 1.09	SS 304	462	35.40 ± 2.16	IG 110	484	79.21 ± 0.11
	470	21.88 ± 0.44		492	35.81 ± 2.63		508	78.93 ± 1.86
	475	13.34 ± 0.32		550	35.82 ± 0.63		554	78.67 ± 4.89
	487	6.60 ± 0.01		571	17.82 ± 3.37		612	83.73 ± 1.92
Mo	468	Not fully molten		614	6.10 ± 0.63	Quartz	471	48.03 ± 0.47
	469	Not fully molten	SS 316	461	45.60 ± 3.90		475	19.08 ± 2.88
	470	7.80 ± 0.01		466	34.30 ± 2.93		477	8.53 ± 0.88
Ta	458	7.87 ± 1.31		474	5.00 ± 0.45		482	5.03 ± 0.47
	460	7.40 ± 1.75						
	467	5.72 ± 0.29						

at similar temperature. This indicated that pure Ni exhibited higher wettability compared to Ni-based alloys. Another set of alloys investigated were Fe-based, *i.e.*, SS 316 and SS 304. SS 316 is composed of lower Cr and higher Ni content, along with the addition of 2 wt% Mo.[29] The larger contact angle measured on SS 304 suggested lower wettability and poorer contact of molten salts with the substrate compared to SS 316.

In general, the wettability of a material is determined by factors such as surface roughness and chemical heterogeneity.[30] In the present study, the impact of surface roughness was negligible as all metal substrates had the same surface finish, as previously mentioned. The varied and complex chemical compositions of the studied substrates, especially for alloys, lead to varied surface energies. It can also vary slightly depending on the crystallographic orientation of the material and the specific conditions under which it is measured. Surface energy directly impacts wettability by determining how readily a liquid spreads on a solid surface. Higher surface energy indicates higher wettability and smaller contact angles. The available surface energy data of studied metal substrates, provided in Table 2, is based on studies of Hodkin *et al.* and Maiya *et al.*[31,32] The smaller surface energy of Mo compared to Ni and Ta corresponds with the larger contact angle measured in this study. However, due to the limited studies on the thermophysical properties of alloys, accurate surface energy data for alloys, including SS 304, SS 316, Alloy 617, and C276, remains scarce and is often presented in broad ranges as shown in Table 2, making it challenging to correlate surface energy with the contact angle.

Regarding LiCl-KCl salt on non-metal substrates, IG 110 exhibited significantly larger contact angles, followed by glassy carbon, MACOR and quartz. LiCl-KCl completely wetted the surfaces of quartz and MACOR starting at 660 °C and 573 °C, with small contact angles of 6.5° and 11.5°, respectively. For IG 110 and graphite, although both are carbon-based materials, LiCl-KCl demonstrated markedly different wettability on these two substrates. Contact angles of LiCl-KCl on glassy carbon decreased from 101.27° at 381

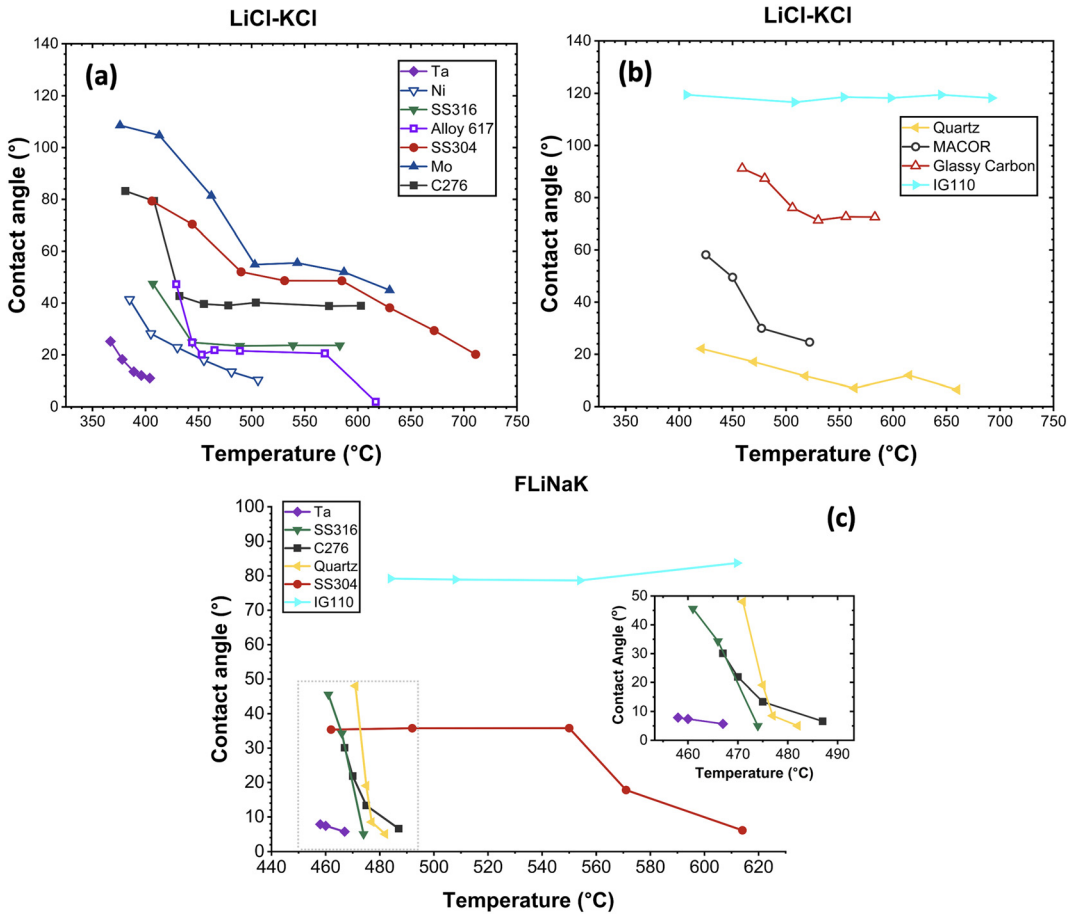

Fig. 4 LiCl-KCl and FLiNaK contact angle change trend with temperature: (a) LiCl-KCl on metal substrates; (b) LiCl-KCl on non-metal substrates; (c) FLiNaK on metal and non-metal substrates.

Table 2 Surface energy of the investigated metal substrates[31,32]

Materials	Mo	Ni	Ta	SS 304	SS 316	Alloy 617	C276
Surface energy (J m^{-2})	2.05	2.34	2.68	1.8–2.5	2.1–2.5	2.0–2.5	2.0–2.5

°C to 72.55° at 583 °C. While on IG 110, the measured contact angles remained consistent at approximately 118° across the studied temperature ranging from 407 °C to 692 °C. The observed difference in wettability can be attributed to the significant variations in their surface microstructures and roughness. Compared to glassy carbon, IG 110 has a more isotropic crystalline structure and a relatively rougher surface.[33] According to the Cassie–Baxter model, the presence of micro-scale geometric features such as grooves, ridges and pits can trap the argon present in the glovebox, leading to a significant increase in the contact angle.[34]

For FLiNaK, the measured contact angles on the studied substrates are generally in the order of $\theta_{IG110} > \theta_{SS\ 304} > \theta_{quartz} > \theta_{C276} > \theta_{SS\ 316} > \theta_{Ta}$, similar to what was observed for LiCl-KCl, except for quartz. Given that all salts underwent identical thermal purification procedures, it was assumed that the potential impact of salt impurities on the contact angle measurements was consistent across both LiCl-KCl and FLiNaK tests. Consequently, the larger contact angles of FLiNaK on quartz was likely due to the difference in substrate surface conditions, such as roughness, since non-metal substrates were not polished to the same finish. All measured contact angles of FLiNaK were less than 90°, indicating high wetting on the substrates. As temperature increased, FLiNaK salt completely wetted all substrates shortly after melting, except for IG 110. The contact angle on IG 110 stabilized around 79° from 484 °C to 612 °C, indicating the lowest wetting potential among all tested substrates.

Regarding the contact angles of both salts measured on the same metal substrates (*i.e.*, Ta, SS 316, SS 304 and C276), the contact angles of LiCl-KCl were greater than those of FLiNaK. According to Young's equation, the contact angle is determined by surface tensions as given in eqn (1), where δ_l, δ_s and δ_{ls} represent the surface tensions of the liquid–gas

phase, solid–gas phase and liquid–solid interfacial surface tension, respectively.[35] The surface tension δ_l of LiCl-KCl and FLiNaK are calculated using the empirical equations δ_l = 189.57 − 0.08 T for LiCl-KCl and δ_l = 272.6 − 0.1014 T for FLiNaK, where T is the temperature in Kelvin and δ_l is the surface tension in dyne cm^{-1}.[36,37] At the given temperature, the surface tension δ_l of FLiNaK is larger than that of LiCl-KCl. In this study, the larger contact angles of LiCl-KCl on the same metal substrates compared to FLiNaK were likely due to the larger surface tension δ_{ls} between LiCl-KCl and the substrate, indicating less wetting.

$$\delta_s = \delta_{ls} + \delta_l \cos\theta \quad (1)$$

$$W_{ls} = \delta_l + \delta_s - \delta_{ls} \quad (2)$$

$$W_{ls} = \delta_l(1 + \cos\theta) \quad (3)$$

Overall, the measured contact angles of both LiCl-KCl and FLiNaK salts decreased as the applied temperature increased. The contact angle is determined by the adhesive force between the molten salt and substrate, and the cohesive force within the molten salt. As the temperature increases, it accelerates ion movements within the molten salts, leading to a decrease in the cohesive force. A smaller cohesive force can result in a smaller contact angle, consistent with the results shown in Fig. 4.

The work of adhesion was calculated using the measured contact angle values. The work of adhesion W_{ls} is the reversible thermodynamic work required to separate the interface of two phases from their equilibrium state to an infinite separation distance.[38] For a liquid–solid phase combination, W_{ls} is defined by eqn (2). By combining eqn (1) and eqn (2), the work of adhesion W_{ls} can be calculated from δ_l and θ as shown in eqn (3). In this study, the calculated work of adhesion is shown in Fig. 5. In LiCl-KCl tests, the work of adhesion initially increased with temperature, then remained constant on most substrates. Except for quartz and IG 110, the calculated work of adhesion on both substrates did not exhibit significant changes within the studied temperature range. Stronger adhesion resulted in a higher potential for molten salts to wet substrates, leading to smaller contact angles, as shown in Fig. 4. In the FLiNaK tests, the salts rapidly and completely wetted most substrates,

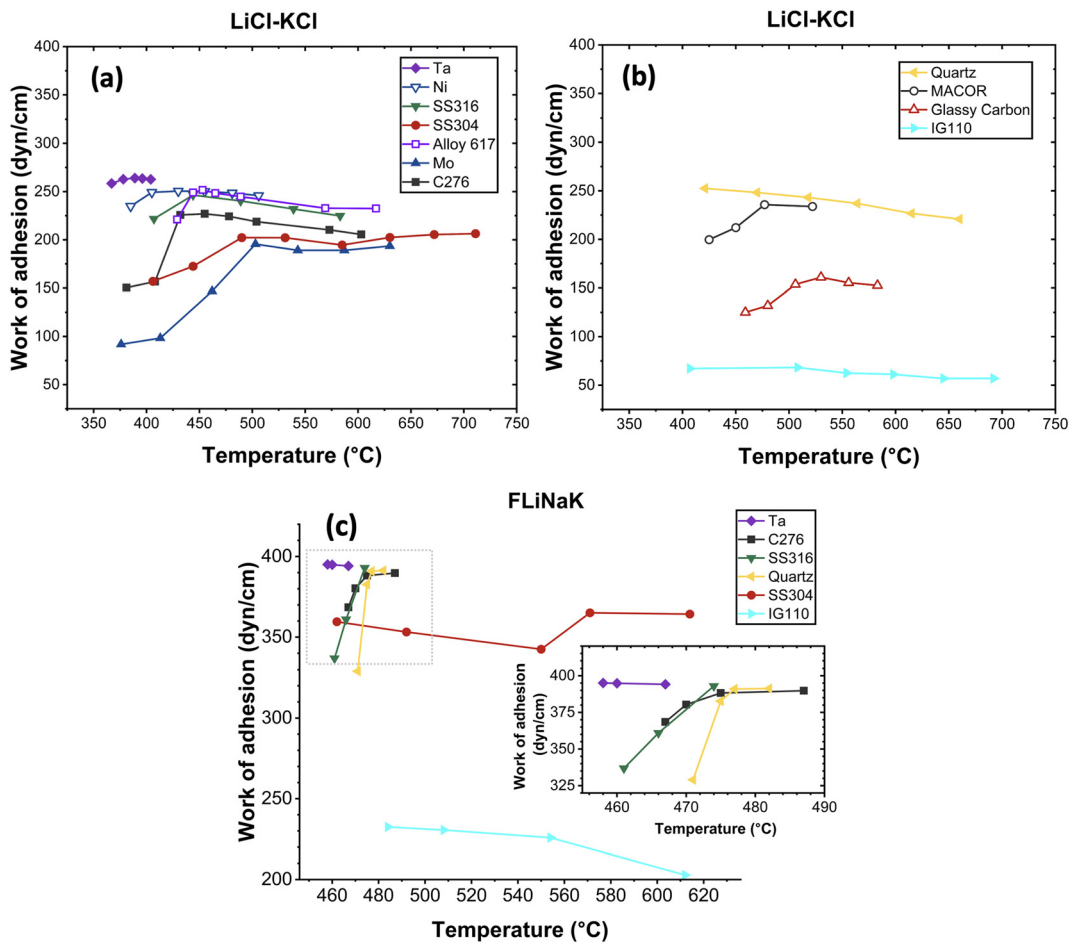

Fig. 5 LiCl-KCl and FLiNaK work of adhesion change trend with temperature on each substrate: (a) LiCl-KCl on metal substrates; (b) LiCl-KCl on non-metal substrates; (c) FLiNaK on metal and non-metal substrates.

resulting in a limited data set that hindered the demonstration of a clear trend. Nevertheless, it is evident that the measured work of adhesion of FLiNaK was larger than that of LiCl-KCl on the same substrates, indicating smaller contact angles, which aligned with Fig. 4.

4. Discussions

As discussed in section 1, contact angle measurement may play a significant role in predicting material corrosion resistance and optimizing the selection of sample container material for DSC analysis. It is well known that the corrosion of structural materials in molten salts initiates at the liquid–solid interface. A smaller contact angle indicates higher wetting, which increases the potential for the salt to interact more effectively with the structural material. This enhanced contact may lead to salt infiltrating the material matrix, consequently resulting in increased corrosion. In case of LiCl-KCl, the contact angle on Mo was the largest among the tested metal substrates, suggesting that Mo may exhibit the best corrosion resistance compared to other metals. The Gibbs free energy of formation ΔG for the reactions $M_{Mo,Ni,Fe,Cr,Ta} + Cl_2 \rightarrow MCl_2$ reactions was calculated using HSC Chemistry 9 software as shown in Fig. 6.[39] Mo has the least negative ΔG, followed by Ni, Fe, Cr and Ta, respectively. In other words, the redox potential of M/MCl_2 (where M = Mo, Ni, Fe, Cr & Ta) follows the sequence Ta, Cr < Fe < Ni < Mo, indicating that Mo has the best corrosion resistance from a thermodynamic standpoint. Furthermore, corrosion studies of Mo-bearing alloys in molten salts have confirmed that Mo within alloys corrodes after Fe, Cr and Nb.[40,41] Therefore, it is feasible to predict the corrosion resistance of pure metals from the contact angle data. Regarding alloys, the measured contact angles of LiCl-KCl and FLiNaK on SS 304 were larger than those on SS 316 in the present study. However, SS 316 is known to possess better corrosion resistance than SS 304 in molten salts.[42] This suggests that the complex chemical compositions of alloys introduce various effects on corrosion from numerous thermophysical properties, making it challenging to use contact angle data alone to predict their corrosion resistance. As observed from our results, predicting corrosion resistance with the assistance of contact angle measurements is primarily applicable to pure metals.

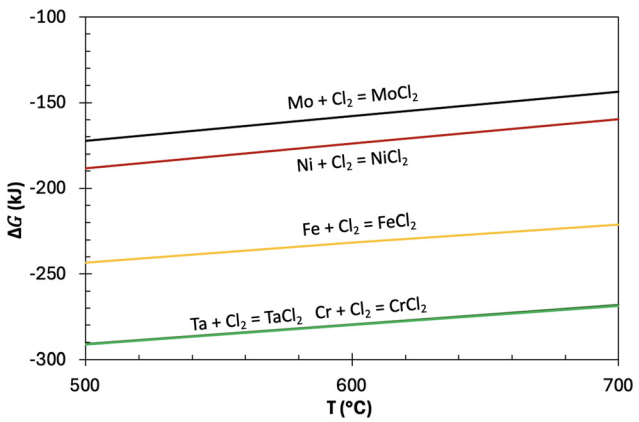

Fig. 6 Gibbs free energy formation of reaction.

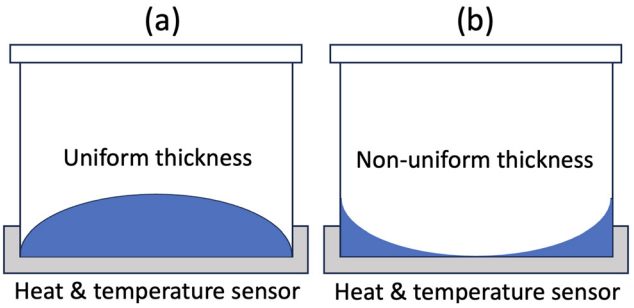

Fig. 7 Molten salt in DSC container. (a) Appropriate contact with uniform thickness; (b) inappropriate contact with non-uniform thickness.

Another potential application of contact angle measurement is the selection of salt container material for DSC measurements. The key to material selection is to ensure proper contact with the container and maintain uniform liquid thickness while preventing the salt from creeping up the container walls during measurements. Therefore, the ideal molten salt condition in the salt container requires the contact angle to be larger than 90°, as illustrated in Fig. 7(a). In this study, the measured contact angles of LiCl-KCl on IG 110 were consistently around 118° from 407 °C to 692 °C, suggesting it to be an excellent container material candidate for DSC measurements within a wide temperature range. In addition, glassy carbon and Mo are also viable options for LiCl-KCl measurements conducted below 480 °C.

Regarding FLiNaK, the measured contact angles were all smaller than 90°, suggesting that none of the tested substrates are an ideal container material. The criteria employed for selecting a DSC container material in this section aim to obtain the most accurate and reliable data in DSC measurements, such as heat capacity and thermal conductivity, for which uniform thickness is crucial. A material with a contact angle larger than 90° is preferred. However, materials with a contact angle less than 90° (40–90°) are acceptable as long as the salt quantity is sufficient and salts remain immobilized in the container.[43–45] This supports the prevalent application of alumina, nickel and platinum containers in DSC measurements.

5. Conclusions

This study has provided comprehensive datasets of contact angle and work of adhesion for LiCl-KCl and FLiNaK salts on a variety of metal and non-metal substrates. Overall, contact angles decrease as temperatures increase. The measured contact angles of both salts follow a similar trend, with IG 110 demonstrating the highest values. FLiNaK exhibits higher wetting than LiCl-KCl across all substrates, likely due to the

higher surface tensions between LiCl-KCl and the substrates. The work of adhesion, calculated from the measured contact angles, aligns with the contact angle trend, showing stronger adhesion at higher temperatures.

The results suggest that contact angle may be a useful predictor of the corrosion resistance of pure metals, with larger contact angles generally indicating better corrosion resistance. However, the correlation may not be as direct for alloys due to their complex chemical compositions. The extensive contact angle database over a wide range of temperatures can also serve as a guide for the selection of salt container material in DSC measurements. It is preferable for the container material to have a contact angle greater than 90° to ensure the most accurate data. However, materials with a contact angle less than 90° (40–90°) could also be acceptable, provided the quantity of salt is sufficient to remain immobile within the container.

Data availability

The data that support the findings of this study are available from the corresponding authors, Qiufeng Yang and Ruchi Gakhar, upon reasonable request.

Author contributions

Qiufeng Yang: writing – original draft, formal analysis, data collection and curation, visualization. Michael Woods: writing – review & editing, methodology, formal analysis, data collection and curation. Ruchi Gakhar: writing – review & editing, resources, project administration, methodology, funding acquisition, conceptualization.

Conflicts of interest

The authors declare no conflicts of interest.

Acknowledgements

This work was supported through Idaho National Laboratory (INL) Laboratory Directed Research & Development (LDRD) program under Department of Energy (DOE) Idaho operations office contract DE-AC07-05ID14517. We thank Christopher Wolfe for his valuable contributions to the initial testing of the contact angle setup. As a summer intern, he was supported by the DOE Office of Science's Science Undergraduate Laboratory Internship program.

References

1 J. W. Kroger, *Fundamentals of High-temperature Corrosion in Molten Salts, ASM Metals Handbook*, ASM International, 2003, vol. 13, pp. 50–55.
2 S. Guo, J. Zhang, W. Wu and W. Zhou, Corrosion in the Molten Fluoride and Chloride Salts and Materials Development for Nuclear Applications, *Prog. Mater. Sci.*, 2018, **97**, 448.
3 J. Serp, M. Allibert, O. Benes, S. Delpech, O. Feynberg, V. Ghetta, D. Heuer, D. Holcomb, V. Ignatiev, J. L. Kloosterman, L. Luzzi, E. Merle-Lucotte, J. Uhlir, R. Yoshioka and D. Zhimin, The Molten Salt Reactor (MSR) in Generation IV: Overview and Perspectives, *Prog. Nucl. Energy*, 2014, **77**, 308.
4 J. W. Ambrosek, Molten chloride salts for heat transfer in nuclear systems, *Ph. D. Dissertation*, University of Wisconsin, Madison, WI, 2011.
5 M. Mehos, C. Turchi, J. Vidal, M. Wagner, Z. Ma, H. Clifford, W. Kolb, C. Andraka and A. Kruizenga, *Concentrating solar power Gen3 demonstration roadmap*, technical report, NREL/TP-5500-67464, 2017.
6 D. Williams, L. Toth and K. Clarno, *Assessment of candidate molten salt coolants for the advanced high-temperature reactor (AHTR)*, ORNL/TM-2006/12, 2006.
7 A. W. Savolainen, *Aircraft nuclear propulsion project quarterly progress report for period ending June 10*, ORNL-2016, Oak Ridge National Laboratory, Oak Ridge, TN, P95, 1956.
8 J. B. Knighton, R. G. Auge and J. C. Brown, *Production tests of single contact molten salt americium extraction process*, CRDL 940501–002, 1970.
9 H. Lee, G. Park and J. Lee, Current status of pyroprocessing development at KAERI, *Sci. Technol. Nucl. Install.*, 2013, **2013**(1), 343492.
10 I. Pioro and R. Duffey, Current and future nuclear power reactors and plants, *Managing Global Warming, An Interface of Technology and Human Issues*, 2019, ch. 4, pp. 117–197, DOI: **10.1016/B978-0-12-814104-5.00004-1**.
11 Y. Grosu, L. Gonzalez-Fernandez, U. Nithiyanantham and A. Faik, Wettability control for correct thermophysical properties determination of molten salts and their nanofluids, *Energies*, 2019, **12**, 3765.
12 P. Hosemann, D. Frazer, M. Fratoni, A. Bolind and M. F. Ashby, Material selection for nuclear applications: challenges and opportunities, *Scr. Mater.*, 2018, **143**, 181–187.
13 T. Chen, A. Moccari and D. Macdonald, Development of controlled hydrodynamic techniques for corrosion testing, *Corros. Eng.*, 1992, **48**, 239.
14 M. Conradi, T. Sever, P. Gregorcic and A. Kocijan, Short- and long-term wettability evolution and corrosion resistance of uncoated and polymer-coated laser textured steel surface, *Coatings*, 2019, **9**, 592.
15 U. Trdan, M. Hocevar and P. Gregorcic, Transition from superhydrophilic to superhydrophobic state of laser textured stainless steel surface and its effect on corrosion resistance, *Corros. Sci.*, 2017, **123**, 21–26.
16 Y. Yuan and T. R. Lee, *Surface Science Techniques*, Springer-Verlag, Berlin, 2013, pp. 3–34.
17 T. Chau, A review of techniques for measurement of contact angles and their applicability on mineral surfaces, *Miner. Eng.*, 2009, **22**, 213–219.
18 H. Yang, Y. Gao and W. Qin, A robust superhydrophobic surface on AA3003 aluminum alloy with intermetallic phases in-situ pinning effect for corrosion protection, *J. Alloys Compd.*, 2022, **898**, 163038.

19 E. Altunbas Şahin, Experimental and theoretical studies of acridine orange as corrosion inhibitor for copper protection in acidic media, *J. Indian Chem. Soc.*, 2021, **99**(3), 100358.
20 V. M. Rangaswamy and J. Keshavayya, Anticorrosive ability of cycloheximide on mild steel corrosion in 0.5M H2SO4 solution, *Chem. Data Collect.*, 2021, **37**, 100795.
21 K. Dahmani, M. Galai and M. Ouakki, Corrosion inhibition of copper in sulfuric acid via environmentally friendly inhibitor (Myrtus communis): combining experimental and theoretical methods, *J. Mol. Liq.*, 2022, **347**, 117982.
22 X. Zhang, M. Zhang and Z. Zhang, Bis-Mannich bases as effective corrosion inhibitors for N80 steel in 15% HCl medium, *J. Mol. Liq.*, 2022, **347**, 117957.
23 Y. Li, Z. Shi, B. Xu, L. Jiang and H. Liu, Bioinspired Plateau-Rayleigh instability on fibers: from droplets manipulation to continuous liquid films, *Adv. Funct. Mater.*, 2024, **34**, 2316017.
24 H. Xu, J. Lin, Y. Zhong, Z. Zhu, Y. Chen, J. Liu and B. Ye, Characterization of molten 2LiF-BeF2 salt impregnated into graphite matrix of fuel elements for thorium molten salt reactor, *Nucl. Sci. Technol.*, 2019, **30**, 74.
25 A. Deepika, B. Abheendra, C. Harish, N. Surendra and G. Meghanath, Wetting and corrosion studies on SS 304 material surfaces, *AIP Conf. Proc.*, 2021, **2317**, 020043.
26 A. Delmore, W. Derdeyn, R. Gakhar and R. Scarlat, *Wetting of graphite by molten fluoride salts: initial experiments*, Transactions of the American Nuclear Society, Philadelphia, Pennsylvania, 2018, vol. 118, pp. 17–21.
27 P. Baumli and G. Kaptay, Wettability of carbon surfaces by pure molten alkali chlorides and their penetration into a porous graphite substrate, *Mater. Sci. Eng., A*, 2008, **495**, 192–196.
28 Q. Yang, J. Ge and J. Zhang, Electrochemical study on the kinetic properties of Fe^{2+}/Fe, Ni^{2+}/Ni, Cr^{2+}/Cr and Cr^{3+}/Cr^{2+} in molten MgCl2-KCl-NaCl salts, *J. Electrochem. Soc.*, 2021, **168**, 012504.
29 **https://www.essentracomponents.com/en-us/news/solutions/access-hardware/304-vs-316-stainless-steel**.
30 H. Eral, D. Mannetje and J. Oh, Contact angle hysteresis: a review of fundamentals and applications, *Colloid Polym. Sci.*, 2013, **291**, 247–260.
31 E. Hodkin, M. Nicholas and D. Poole, The surface energies of solid molybdenum, niobium, tantalum and tungsten, *J. Less-Common Met.*, 1970, **20**, 93–103.
32 P. Maiya and J. Blakely, Surface self-diffusion and surface energy of nickel, *J. Appl. Phys.*, 1967, **38**, 698–704.
33 T. Weilert, K. Walton, S. Loyalka and J. Brockman, Europium diffusion in IG-110 nuclear graphite, *J. Nucl. Mater.*, 2022, **561**, 153544.
34 S. Riahi, B. Niroumand, A. Moghadam and P. Rohatgi, Effect of microstructure and surface features on wetting angle of a Fe-3.2 wt% C.E. cast iron with water, *Appl. Surf. Sci.*, 2018, **440**, 341–350.
35 N. Eustathopoulos, M. G. Nicholas and B. Drevet, *Wettability at High Temperatures*, Pergamon, Elsevier Science Ltd, Oxford, UK, 1999.
36 G. Janz, R. Tomkins and C. Allen, Molten salts: Volume 4, part 2, chlorides and mixtures-electrical conductance, density, viscosity, and surface tension data, *J. Phys. Chem. Ref. Data*, 1975, **4**, 871.
37 M. Sohal, M. Ebner, P. Sabharwall and P. Sharpe, Engineering database of liquid salt thermophysical and thermochemical properties, INL/EXT-10-18297, 2010.
38 S. Ebnesajjad and A. Landrock, Chapter: surface tension and its measurement, *Adhesives Technology Handbook*, 3rd edn, 2015.
39 HSC Chemistry 9, Metso Finland Oy.
40 O. Muransky, C. Yang, H. Zhu, I. Karatchevtseva, P. Slama, Z. Novy and L. Edwards, Molten salt corrosion of Ni-Mo-Cr candidate structural materials for molten salt reactor (MSR) systems, *Corros. Sci.*, 2019, **159**, 108087.
41 W. Phillips, Z. Karmiol and D. Chidambaram, Effect of metallic Li on the corrosion behavior of Inconel 625 in molten LiCl-Li2O-Li, *J. Electrochem. Soc.*, 2019, **166**, C162–C168.
42 R. Bradshaw and S. Goods, *Corrosion resistance of stainless steels during thermal cycling in alkali nitrate molten salts*, Sandia report, SAND2001–8518, 2001.
43 B. Munoz-Sanchez, J. Nieto-Maestre, G. Imbuluzqueta, I. Maranon, I. Iparraguirre-Torres and A. Garcia-Romero, A precise method to measure the specific heat of solar-based nanofluids, *J. Therm. Anal. Calorim.*, 2017, **129**, 905–914.
44 M. Thoms, Adsorption at the nanoparticle interface for increased thermal capacity in solar thermal systems, *PhD thesis*, Massachusetts Institute of Technology, Cambridge, MA, USA, 2012.
45 G. Hohne, W. Hemminger and H. Flamersheim, *Differential scanning calorimetry*, Springer-Verlag Berlin Heidelberg GmbH, 2nd edn, 2003, **https://link.springer.com/content/pdf/10.1007/978-3-662-06710-9**.